

ENVIRONMENTAL STUDIES

Unequal exposure to heatwaves in Los Angeles: Impact of uneven green spaces

Yi Yin^{1*}, Liyin He^{1†}, Paul O. Wennberg^{1,2}, Christian Frankenberg^{1,3}

Cities worldwide are experiencing record-breaking summer temperatures. Urban environments exacerbate extreme heat, resulting in not only the urban heat island but also intracity variations in heat exposure. Understanding these disparities is crucial to support equitable climate mitigation and adaptation efforts. We found persistent negative correlations between daytime land surface temperature (LST) and median household income across the Los Angeles metropolitan area based on Ecosystem Spaceborne Thermal Radiometer Experiment on Space Station observations from 2018 to 2021. Lower evapotranspiration resulting from the unequal distribution of vegetation cover is a major factor leading to higher LST in low-income neighborhoods. Disparities worsen with higher regional mean surface temperature, with a \$10,000 decrease in income leading to ~0.2°C LST increase at 20°C and up to ~0.7°C at 45°C. With more frequent and intense heat waves projected in the future, equitable mitigation measures, such as increasing surface albedo and tree cover in low-income neighborhoods, are necessary to address these disparities.

INTRODUCTION

Heat extremes pose a substantial threat to public health, as they increase mortality and morbidity (1), reduce physical work capacity (2), and negatively affect mental health (3). One of the major factors that exacerbate this risk in cities is the urban heat island effect, which refers to the phenomenon that urban areas are typically warmer than their surrounding suburban and rural areas (4). This phenomenon results from several factors, including the heat-absorbing properties of building materials such as concrete, a lack of vegetation, heat generated from human activities, and the city geometry, which traps heat and reduces ventilation due to the close proximity of tall buildings (5). Characteristics of the built environment, such as city geometry, green space, and surface reflectance, play a critical role in not only creating the urban heat island effect compared to rural areas but also resulting intracity variations (6). The high temperatures in urban centers intensify energy consumption, with waste heat further amplifying the challenges, putting vulnerable populations at risk (7).

As of 2020, 56% of the world's population lives in urban areas, and urbanization is still a fast-ongoing process in developing countries (United Nations Population Division). Projections suggest that the fraction of the world population living in urban areas will reach nearly 70% by 2050. Accompanying this rural-to-urban demographic shift is a warming climate (8), with the enhancement of heat waves in terms of frequency, intensity, and duration (5). Given the increasing risks associated with urban heat extremes, it is becoming increasingly crucial for cities to develop strategies to reduce heat exposure. Therefore, it is important to understand heat exposure experienced by different communities in urban areas where the built environment amplifies extreme heat.

The impacts of climate change can exacerbate existing inequalities in society (9), such as uneven distribution of vegetation and tree canopy cover (10, 11), urban heat islands (12–14), and environmental hazards and pollutants (15, 16). Disparities in heat exposure have been observed across major U.S. cities, where resource-limited residents and communities of color tend to live in areas with the highest exposure to heat waves (12–14). Hoffman *et al.* (12) found that, across 108 U.S. urban areas, 94% of studied urban areas display consistent patterns of elevated land surface temperatures (LSTs) in formerly redlined areas relative to their non-redlined neighbors, demonstrating the long-lasting impacts of historical housing policies. Hsu *et al.* (14) found that people of color and those living in poverty experience greater heat exposure in comparison to non-Hispanic whites and households above two times the poverty line, respectively, across 175 U.S. cities. These results highlight the disparities in heat exposure among different racial and socioeconomic groups in the United States, underscoring the urgent need for detailed information about the sources of these disparities in current urban settings to support equitable adaptation and mitigation efforts.

In this study, we focus on Los Angeles (LA) County, currently home to 9.8 million residents with diverse cultural and socioeconomic backgrounds (U.S. Census Bureau, 2021, <https://www.census.gov/quickfacts/fact/table/losangelescountycalifornia,CA/PST045221>). Previous studies have shown that the case of urban heat islands in LA is uniquely complex because of various topographical features and oceanic influences (17, 18). To understand the temporal and spatial variations of urban heat distribution, we use LST measurements from Ecosystem Spaceborne Thermal Radiometer Experiment on Space Station (ECOSTRESS) (18, 19). ECOSTRESS measures high-resolution (~70 m) LST at various local times throughout the year, providing an opportunity to understand the diurnal and seasonal variations in heat exposure patterns. We first analyze the relationships between ECOSTRESS LST and socioeconomic status across different neighborhoods from July 2018 to September 2021, covering four summers from 2018 to 2021 with a few notable heatwaves. Further, we analyze the impacts of surface

Copyright © 2023 The Authors, some rights reserved; exclusive licensee American Association for the Advancement of Science. No claim to original U.S. Government Works. Distributed under a Creative Commons Attribution NonCommercial License 4.0 (CC BY-NC).

¹Division of Geological and Planetary Sciences, California Institute of Technology, Pasadena, CA, USA. ²Division of Engineering and Applied Science, California Institute of Technology, Pasadena, CA, USA. ³Jet Propulsion Laboratory, California Institute of Technology, Pasadena, CA, USA.

*Corresponding author. Email: yinyi11@gmail.com

†Present address: Department of Global Ecology, Carnegie Institution for Science, Stanford, CA, USA.

albedo, vegetation coverage, and evapotranspiration (ET) on the heat exposure pattern to identify potential directions for equitable climate mitigation and adaptation efforts.

RESULTS

Negative correlations between LST and income

An analysis of a typical summer mid-day observation from the ECOSTRESS satellite on 4 June 2021, at 1 p.m. reveals a noteworthy negative correlation between LST and median household income across the LA County defined at the zip code level ($r = -0.68$, $P < 0.01$; Fig. 1A). This negative correlation is also evident at a finer spatial resolution at the block group level ($r = -0.63$, $P < 0.01$; fig. S2A), as well as at the ECOSTRESS LST pixel level when we apply the block-group level income data to corresponding location ($r = -0.61$, $P < 0.01$; figs. S1 and S2B). The range of neighborhood average LST spans from 36° to 54°C along the income spectrum, representing a difference of almost 20°C (Fig. 1, A and D).

Accompanying this negative correlation between LST and income, we also observe a positive correlation between ET and

income ($r = 0.62$, $P < 0.01$; Fig. 1B). For reference, the downward solar shortwave radiation reaching the land surface is 963 W m⁻² at the time of measurement. Hence, the highest ET rate we observe could dissipate nearly a third of the incoming radiation. The ET and LST retrievals are based on ECOSTRESS observations and are negatively correlated as expected ($r = -0.7$, $P < 0.01$; fig. S3A): Higher ET leads to more latent heat loss and, hence, lower LST. LA is located in a semiarid region with a long dry season each year, limiting vegetation growth during summer months due to limited water availability (20). High vegetation cover is often maintained through irrigation, which supports ET and helps to cool the land surface (21). This is evidenced by the significant correlation between normalized difference vegetation index (NDVI) derived from Landsat reflectance and ECOSTRESS ET ($r = 0.61$, $P < 0.01$; fig. S3B).

The strong correlations between income, NDVI, ET, and LST suggest that neighborhoods with higher income levels generally have higher NDVI, higher ET, and, hence, lower LST. We used linear regression to infer the slopes of LST change against income as the sensitivity of LST to income gradient, which measures the

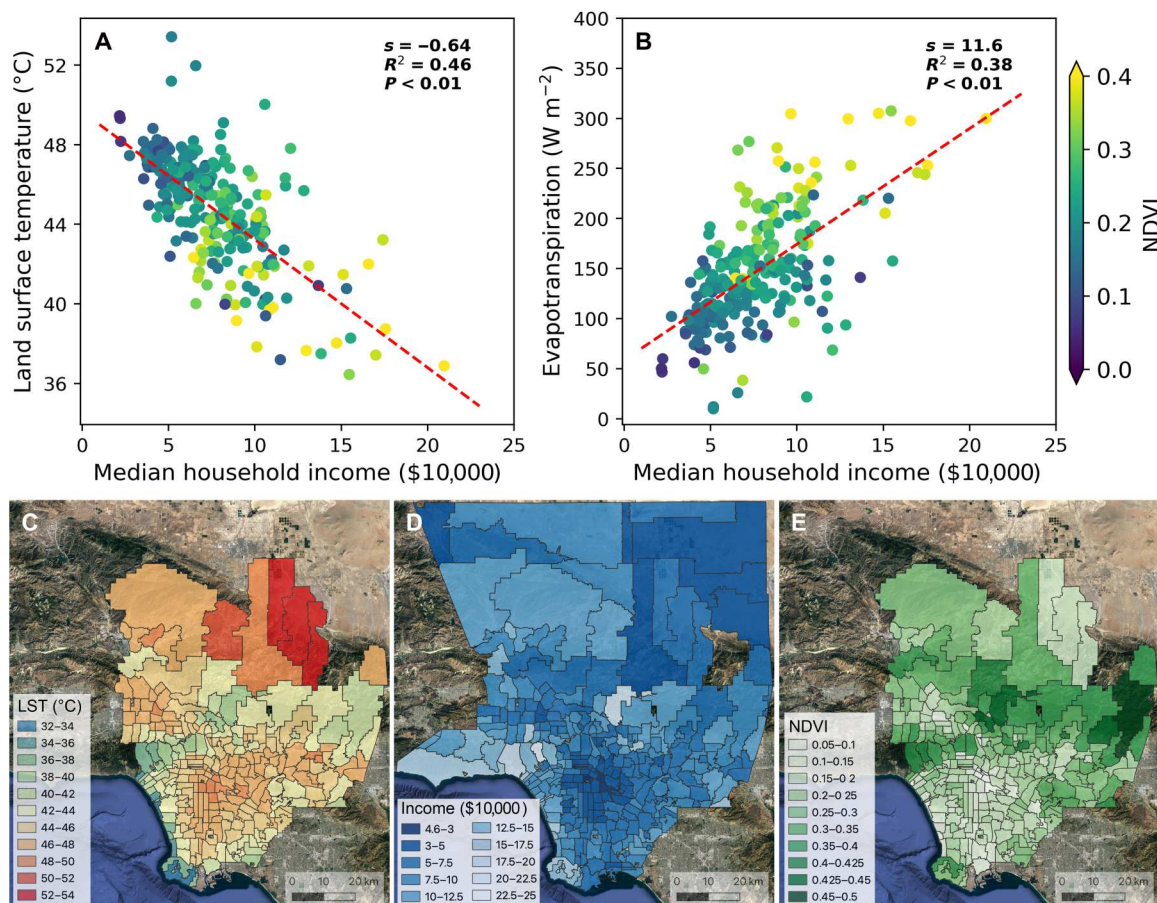


Fig. 1. Spatial patterns and correlations of LST, median household income, and vegetation greenness across the LA County. LST data are from ECOSTRESS captured at 1 p.m., 4 June 2021; 2019 median household income data are from U.S. Census database; normalized difference vegetation index (NDVI) is from Landsat 8 averaged over June 2021. (A) Correlations between median household income and LST. (B) Correlations between median household income and instantaneous ET. Each dot in (A) and (B) represents a ZIP Code Tabulation Area (ZCTA). Corresponding spatial distributions of (C) ECOSTRESS LST, (D) census median household income, and (E) Landsat NDVI at the zip code level. Note that only neighborhoods with valid observations passing all the filtering processes as documented in the Materials and Methods are shown in the NDVI and LST distribution plots.

degree of disparity. For example, in Fig. 1A, we derived a slope of -0.64 ($^{\circ}\text{C}/\$10,000$), which indicates that for every decrease of $\$10,000$ in the annual household income across various neighborhoods, there is an increase of 0.64°C in LST. To assess the robustness of the relationships identified, we tested different administrative boundaries of the LA area here, including the larger LA metropolitan area, the South Coast Air Basin that contains all of Orange County, and the nondesert regions of LA County, Riverside County, and San Bernardino County, as well as the nondesert regions of LA County. Similar negative correlations between LST and income are found, and the results are not sensitive to the choice of administrative boundaries. Therefore, we present results using the boundary of nondesert regions of LA County hereafter to reduce differences due to natural geographical settings. Besides, we estimated the impacts of geographic settings in terms of altitude, slope aspects, and distance to the nearest coast; the first two factors do not appear to play a significant role in influencing the observed LST pattern, while the distance to the nearest coast has a minor effect ($r^2 = 0.1$; fig. S5).

Temporal variations of the LST and income relationships

We collect all available ECOSTRESS data that cover more than 30% of the ZIP Code Tabulation Areas (ZCTAs) in the LA County from July 2018 to September 2021 at various local times to capture diurnal and seasonal variations in heat exposure patterns. We have a total of 329 ECOSTRESS LST images that passed all quality checks with a near uniform distribution of the diurnal

sampling (sampling numbers are shown in Fig. 2C). We find consistent negative correlations between daytime LST and median household income (Figs. 2 and 3), which demonstrates the persistence of the observed disparity in LST across income as shown in the case presented in Fig. 1.

The sensitivity of LST to income is greatest around noon (Fig. 2A). At night (defined as 9 p.m. to 8 a.m.), the correlation between LST and median household income is generally insignificant, although it is still negative. The correlation becomes significantly negative from 9 a.m. onward, peaking at 1 p.m., and thereafter decreases gradually in the late afternoon (Fig. 2B). A strong positive correlation between LST and shortwave albedo is also observed during the daytime (fig. S4), which suggests that higher albedos are associated with higher LST—the opposite of what we would expect if albedo were the main factor affecting the surface energy budget. Therefore, we conclude that ET is the dominant term shaping the regional disparities of LST across income groups. The diurnal variations of the disparity generally follow the diurnal cycle of solar radiation—in the morning, as the incoming solar radiation surpasses the outgoing longwave radiation, surface temperatures start to increase. Only areas with vegetation cover and sufficient soil water content can dissipate heat through ET and result in a lower LST. As the sun starts to set, photosynthesis and ET rates decline, and the differences in LST across income groups become smaller.

The daytime patterns of the derived sensitivity of LST to income show the most negative values (i.e., the largest disparities) during

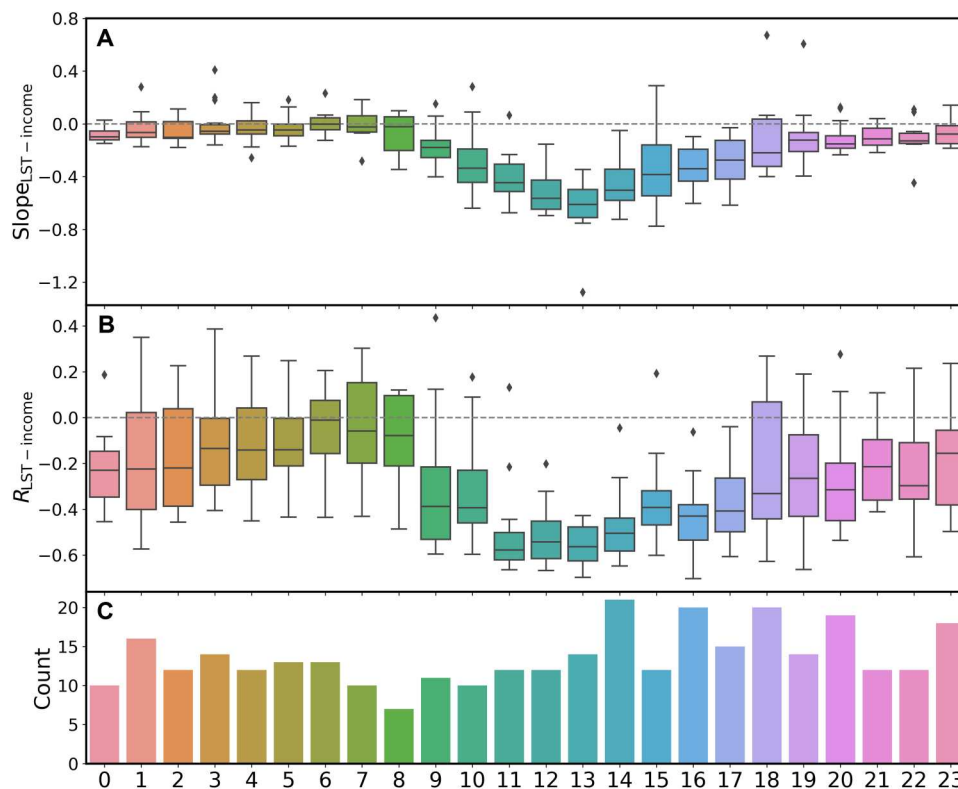


Fig. 2. Diurnal distribution of observed disparities. (A) Slopes of LST against income, (B) correlation coefficients between LST and income, and (C) number of ECOSTRESS images analyzed. Each box shows the quartiles of the dataset, while the whiskers extend to show the rest of the distribution, except for diamonds that are detected as outliers.

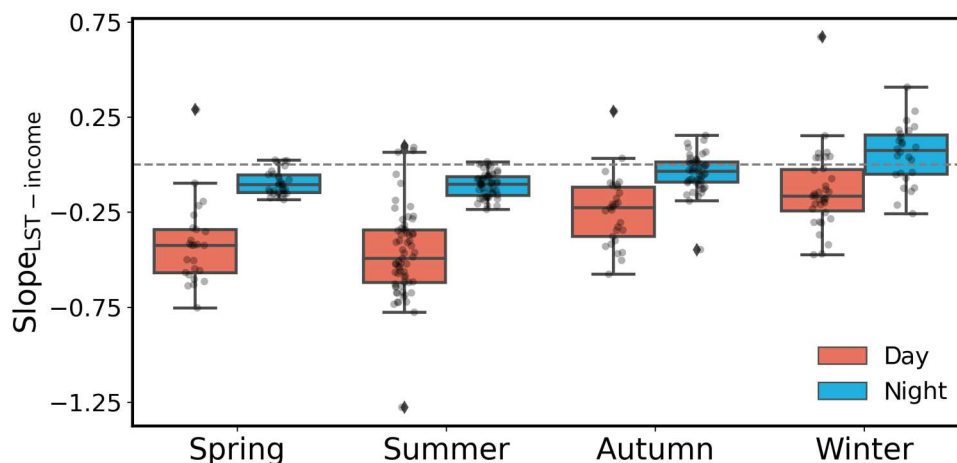


Fig. 3. Seasonal distribution of slopes derived from ECOSTRESS LST (°C) against annual household income (\$10,000), a measure for the magnitudes of disparities in heat exposure among different income groups. The individual light grey dot represents one overpassing image being analyzed. Each box shows the quartiles of the dataset, while the whiskers extend to show the rest of the distribution, except for diamonds that are determined as outliers.

summer (June, July, and August) and spring (March, April, and May) (Fig. 3). This is consistent with the seasonal dynamics of photosynthesis in this area, where photosynthesis peaks from mid-spring (~April) to late summer (~August) following the dynamics of solar radiation and water availability (20). In autumn and winter, the magnitude of disparity decreases markedly as photosynthesis declines, confirming the important role of ET in driving the spatial differences in LST. The LST and income correlations and slopes are mostly negative, except for a slightly positive slope and correlation during winter nights.

The correlation coefficient between LST and median household income is slightly positive when the regional mean LST is low, and it gets more negative with rising LST from 0° to 30°C and remains relatively stable beyond that, suggesting persistent patterns of disparity in heat exposure at high temperatures (Fig. 4A). However, the magnitude of observed disparities across all the ECOSTRESS images—as measured by the slopes of the LST, income regression—continues to increase with rising temperatures, indicating a higher

disparity in heat exposure among income groups under global warming (Fig. 4B).

Impacts of albedo on LST

Albedo, which represents the fraction of the incoming radiation that is reflected by a surface, plays a significant role in the surface energy budget. While our analysis revealed that the spatial pattern of LST is predominantly shaped by ET, we focus on impervious surfaces of the built environment to evaluate the impacts of albedo on LST in the absence of vegetation impacts. To define built surfaces, we used three criteria: classified as urban in the Landsat land use/land cover classification, an NDVI of <0.01 (to remove possible vegetation), and an albedo of >0.1 (to remove water surface). We used quantile regression to fit the conditional quantiles of the LST response to albedo values (Fig. 5A). This method effectively minimizes the influence of other factors that may affect LST, such as emissivity, heat conductance, and heat capacity. The analysis suggests that higher albedo values are generally associated with lower

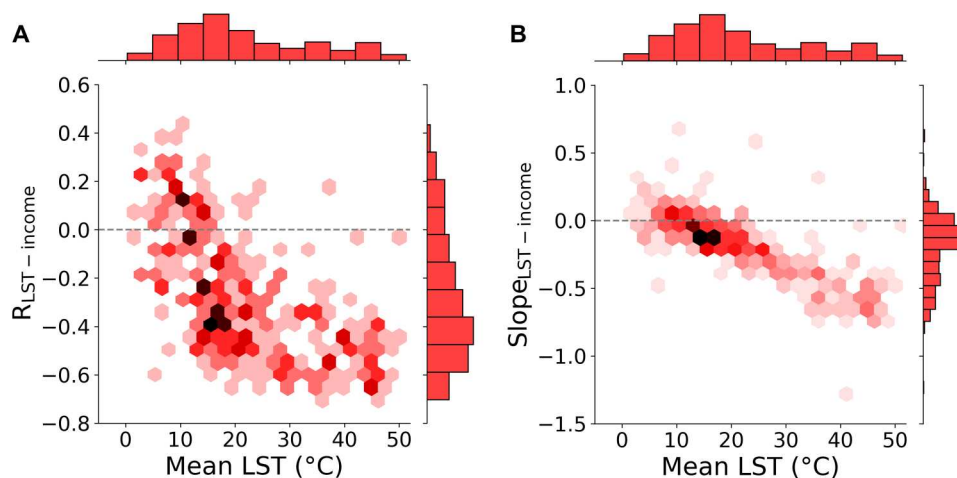


Fig. 4. Enhancing correlation and magnitudes of disparity with rising surface temperature. Two-dimensional density distribution of (A) correlation coefficients between LST with median household income (y axis) and regional mean LST (x axis) and (B) slopes of LST against income (y axis) and the regional mean LST (x axis).

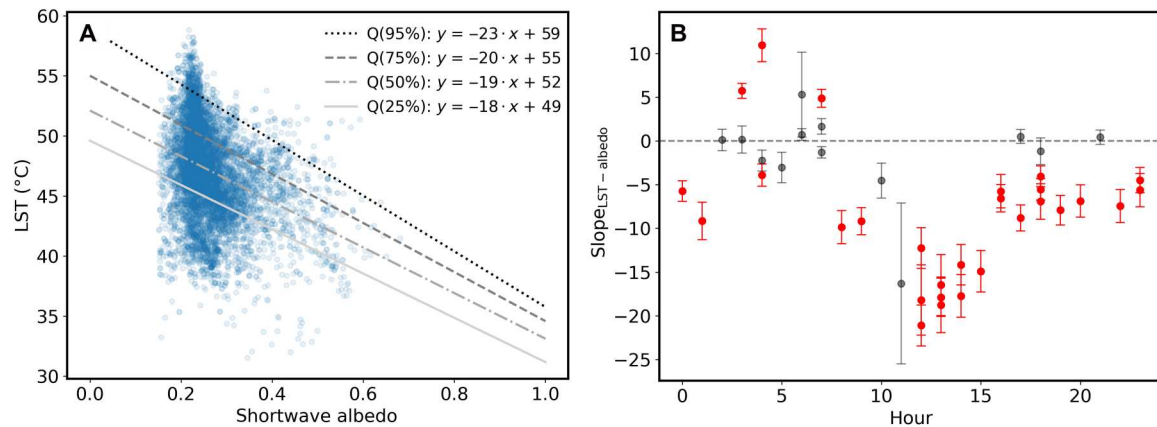


Fig. 5. Correlation between LST and shortwave albedo over urban nonvegetative built surfaces. (A) Quantile regression of ECOSTRESS LST against Landsat effective shortwave surface albedo. The ECOSTRESS data are the same as shown in Fig. 1. Each dot represents a collocated pixel. All quantile regressions shown are statistically significant ($P < 0.01$). (B) Diurnal variations of the slopes derived from 95% quantile regression at different local times in the summer of 2018. Slopes that are statistically significant ($P < 0.01$) are shown in red in (B).

LST ($P < 0.01$ for all quantile regressions shown in Fig. 5A). The steeper slopes observed in higher quantiles provide valuable insights into the upper tails of the LST distribution. The diurnal variations in the LST-albedo slopes suggest that the variations in LST due to albedo are most prominent around noon when solar radiation is the strongest (Fig. 5B), which further corroborates our finding.

This analysis provides us with an empirical reference for the sensitivity of LST to changes in albedo. Specifically, it implies that an increase of 0.1 in albedo could potentially lead to a decrease of around 2°C in LST at noon. In July, a typical daily mean solar radiation in LA is about 340 W m^{-2} , and an increase of 0.1 in the surface albedo could lead to a reduction of absorbed energy by 34 W m^{-2} . This reduction is equivalent to the latent heat loss through the ET of 1.23 mm day^{-1} at a surface temperature of 40°C (1.21 mm day^{-1} at 30°C). This is a simplified estimation of the magnitude of expected effects and more sophisticated modeling approaches are clearly necessary to fully understand the effects of albedo change.

DISCUSSION

Implications of the observed LST patterns

While our findings corroborate earlier studies that document disparities in surface temperature in major U.S. cities (12, 14), this analysis advances upon these by identifying robust linear correlations between median house income and daytime LST across LA at 70-m pixel level, block group level, and zip code level using spatial analysis based on high-resolution LST observations from ECOSTRESS. We find that vegetation cover, which correlates with neighborhood household income due to historical and contemporary inequities, is the most significant driving factor in explaining the observed LST variations, with much more explaining power than topographic features such as distance to the nearest coast or elevation and slope aspects (fig. S5).

The case of unequal heat exposure in the LA area is particularly prominent, as the city locates in a semiarid environment with a significant dry season, where most urban vegetation requires irrigation in summer. This results in disparities in LST that reflect disproportionately higher outdoor water usage in neighborhoods with higher income. Previous studies have shown that, across the United States,

Southeast and Western cities exhibit the greatest intracity differences in LST between areas with different historical housing policies (12). These spatial differences could be related to different background climates that have a strong influence on the intensity of urban heat islands (22). To further understand regional patterns of this important aspect of climate and environmental justice, additional studies are urgently needed to expand the scope of our analysis.

One important limitation of this study is that remotely sensed LST is “skin temperature,” which is only representative of the surface layer of buildings or trees and may not reflect the ambient temperature one experiences within a building interior or under a canopy understory. In particular, LST does not represent the shading effects from trees in the canopy understory; hence, the cooling effect of tree canopy is likely underestimated using the LST metrics. Urban mobile platform observations have shown that daytime air temperature decreases nonlinearly with increasing canopy cover (23). A case study in Sacramento, California, suggests that shade trees can yield seasonal cooling energy savings of ~30% for residential houses (24).

To complement the LST analysis, we also used a gridded daily temperature dataset at 4-km resolution that is interpolated from meteorological stations at 4-km resolutions using the PRISM (Parameter-elevation Relationships on Independent Slopes Model) product (25). ECOSTRESS LST at noon is significantly correlated with the same day PRISM daily max air temperature at zip code level, and the range of differences across neighborhoods in terms of 2-m air temperature and LST is comparable, both around 20°C , although LST has higher absolute values (fig. S6A). The regression of mean daily maximum temperatures in summer months against median household income is not statistically significant (fig. S6B). However, there are huge limitations in using interpolated air temperature at a 4-km spatial resolution to represent spatial variations in urban heat exposure adequately. Hence, fine-scale LST observations can still provide valuable insights into intracity temperature gradients and complexities at detailed levels that are difficult to achieve with meteorological temperature data alone. Moving forward, more urban-scale in situ observations of air

temperature and other relevant meteorological variables are urgently needed to better understand urban heat exposure (26).

Possible mitigation methods

Larger disparities in LST are observed as temperature increases (Fig. 4), which indicates that the observed disparities are likely to worsen under future warming unless effective mitigation efforts are put into place. Therefore, we propose the following mitigation methods based on our findings that underscore the importance of vegetation cover, evapotranspirative cooling, and surface albedo.

Increase green spaces and greywater recycling

Planting trees and vegetation are effective nature-based solutions to mitigate urban heat island and moderate urban microclimates through shading and ET (23). However, vegetation requires sufficient water to maintain its health and cooling capacity, but water resources are limited in the semiarid environment of LA. Therefore, it is crucial to strategically locate trees in neighborhoods with high vulnerability and plan for their sustainable irrigation to ensure continued success. Previous studies found that turfgrass accounts for around 70% of ET from vegetation in LA (27), and overwatering of residential landscapes is observed (28). In contrast, mature trees could access groundwater to complement shallow water from irrigation (29). Therefore, there is great potential to support more tree canopies in the LA area by shifting from water-consuming turfgrass into drought-tolerant trees with thoughtful planning and allocating necessary water resources to the underserved communities. In the meantime, promoting green landscapes and reducing impervious surfaces can increase the ground's capacity to absorb rainwater. Implementing rain gardens, swales, and underground infiltration trenches can capture, treat, and naturally recharge groundwater, thereby augmenting local water supplies (30). As a cobenefit, these practices could partially help mitigate flooding risks that are disproportionately higher for the disadvantaged populations (31, 32).

To reduce the demand for additional irrigation, promoting efficient use of water already delivered to homes through greywater recycling for landscapes can be a viable option. Previous studies have found that 50 to 80% of household wastewater can be classified as greywater, and greywater recycling can positively affect the environment (33–35). In 2015, LA Department of Water and Power reported an average residential water usage of 338 million gallons per day (36). Assuming that 70% of this water is used indoors (37), if 50% of the greywater is recycled for landscape irrigation and evenly spread over the service area of 473 square miles, then we could expect an added ET of approximately 0.35 mm day^{-1} , equivalent to 30% of the average daily precipitation over this area. However, proper care and maintenance are crucial to ensure environmental safety.

Solar-reflective cool pavements and roofs

As it takes time for trees to mature and provide effective shading and cooling effects (10), using reflective surfaces, such as rooftops, exterior walls, and pavements could provide some immediate effect to cool urban areas (38). Pavements and roofs typically constitute over 60% of urban surfaces (roofs, 20 to 25%; pavements, about 40%) (39). Using reflective materials, roof and pavement albedos can be increased by about 0.25 and 0.15, respectively, resulting in a net albedo increase for urban areas of about 0.1 (39). Simulations using coupled Earth System Model show that altering the surface

albedo could cool not only the LST but also the surface air temperature in many urbanized areas across the globe (40), with considerable cobenefits to air quality (41). The LA county has made cool roofs mandatory (<https://file.lacounty.gov/SDSInter/bos/supdocs/128172.pdf>), and a novel approach to adding a reflective coating on pavement has been applied in high-vulnerability neighborhoods with projects such as Cool LA led by the LA Bureau of Street Services (<https://streetsla.lacity.org/cool-la-neighborhoods>, last access on 16 August 2022). While the effects of cool roofs have been well studied, future studies are needed to assess the overall thermal and environmental effects of cool pavement beyond its effect on surface temperature, as increasing the surface albedo for walkways can reflect more solar radiation and alter the energy budget of the near surface ambient air in areas of human activity (42).

Increasing awareness and system resilience

It is critical to identify the most vulnerable groups and allocate sufficient resources to adapt to climate risks, as climate adaptation competes with other priorities for government and stakeholders. Although our study focuses on the case of LA, it is essential to note that increasing temperate cities, unaccustomed to heatwaves, are also experiencing rising heat extremes, as seen in the deadly heatwave that occurred in the United Kingdom in 2022 (43). The heat exposure inequity metric developed in this study can help identify vulnerable communities in other cities with different background climates, guiding appropriate mitigation efforts. Raising awareness about the risks of heatwaves and acknowledging the unequal exposure across different socioeconomic groups are increasingly important. This can encourage urban planning choices and prompt homeowners to take action through city programs and other incentives to promote environmental justice and increase the resilience of our cities as summers get warmer.

MATERIALS AND METHODS

ECOSTRESS LST and ET

The ECOSTRESS was launched to the International Space Station (ISS) on 29 June 2018, which provides by far the highest spatial resolution thermal infrared data available from space between $\sim 52^\circ\text{N}$ and $\sim 52^\circ\text{S}$ (38-m along-track and 69-m across-track). Unlike typical sun-synchronous orbits, the precessing ISS orbit allows more dynamic sampling, allowing for an overpass return frequency to be 1 to 5 days for a given location (depending on the latitude) at different local times, with revisits around the same local time approximately every 60 days (19). Such a unique diurnal sampling strategy of ECOSTRESS allows us to gain more insights into the nature of temporal variation in urban heat island effects at fine spatial scales.

We use ECOSTRESS level 2 LST retrievals (ECO2LSTE v001, available at <https://lpdaac.usgs.gov/products/eco2lste/v001/>) from July 2018 to September 2021. For each scene, we apply corresponding cloud masks and quality flags to ensure that only "normal quality" pixels are used in further analysis. Clear-sky ECOSTRESS LST retrievals have been evaluated with ground-based measurements with an average root mean square error of 1.07 K, a mean absolute error of 0.4 K, and $R^2 > 0.988$ across 14 sites with different landcover types (44). A systematic evaluation of different satellite LST products against ground observations for agricultural

landscapes in the U.S. Cron Belt suggests that ECOSTRESS data show the highest accuracy in daytime LST (45). ECOSTRESS level 3 ET retrievals (ECO3ETPTJPL v001, <https://lpdaac.usgs.gov/products/eco3etptjplv001/>) are also used in accordance with LST retrievals (19, 46).

Landsat 8 shortwave reflectance

Landsat 8 provides surface reflectance retrievals at 30-m resolution over each 16-day period. We follow the user guide to apply pixel quality (QA_PIXEL) and radiometric saturation quality assessment (QA_RADSAT) flags for quality filtering (see Landsat 8 user guide https://d9-wret.s3.us-west-2.amazonaws.com/assets/palladium/production/s3fs-public/atoms/files/LSDS-1574_L8_Data_Users_Handbook-v5.0.pdf). QA_PIXEL includes several tags, e.g., clear, water, snow, cloud, cloud shadow, etc. Only pixels with no dilated cloud, no cirrus, no cloud, and no cloud shadow are used in the analysis. In addition, we exclude pixels with saturation in either shortwave or thermal bands.

The effective surface shortwave albedo is calculated on the basis of the eight Landsat operational land imager surface reflectance bands using an empirical method that focuses specifically on urban conditions (47). We also use the NDVI, a commonly used proxy for vegetation greenness to represent the relative abundance of vegetation on the land surface. We temporally aggregate Landsat data to generate monthly values for further analysis.

Socioeconomic and demographic statistics

Socioeconomic and demographic status have many aspects, such as income, age distribution, and racial and ethnic composition. Here, we focus mostly on income as a proxy for each neighborhood's resources to deal with environmental stresses. We use median household income (in 2019 inflation-adjusted U.S. dollars) from the American Community Survey 2015 to 2019 5-Year Data (available at www.census.gov/newsroom/press-releases/2020/acs-5-year.html). The cartographic boundary of ZCTAs was accessed from the census database (www.census.gov/geographies/mapping-files/time-series/geo/carto-boundary-file.html).

Analyzing the correlation between LST and income at various times

For each scene of the ECOSTRESS LST overpass covering LA County, pixels passing the cloud screen and quality flags are used for further analysis. We calculate average and median LST over individual ZCTAs when more than 60% of the ZCTA areas are covered by valid data to ensure the representativeness of the average LST. We also exclude ZCTAs with a population of fewer than 1000 people and ZCTAs where the calculated median LST deviated more than three times the regional SD from the regional median to avoid outliers. For each ECOSTRESS scene, if the aggregated data cover more than 30% of the ZCTAs, then we keep them for further statistical analysis. We have a total of 329 ECOSTRESS LST images that passed these quality checks with a near uniform distribution of the diurnal sampling (sampling numbers are shown in fig. S4C). Further, we analyze the statistical relationships between LST and income and estimate the sensitivity of LST to income gradient using the ordinary least squares regression. For the filtering process at both zip code and overpass levels, we tested various thresholds for minimum data coverage, and they do not result in significant changes of the results.

Supplementary Materials

This PDF file includes:

Figs. S1 to S6

[View/request a protocol for this paper from Bio-protocol.](#)

REFERENCES AND NOTES

1. K. L. Ebi, A. Capon, P. Berry, C. Broderick, R. de Dear, G. Havenith, Y. Honda, R. S. Kovats, W. Ma, A. Malik, N. B. Morris, L. Nybo, S. I. Seneviratne, J. Vanos, O. Jay, Hot weather and heat extremes: Health risks. *Lancet* **398**, 698–708 (2021).
2. J. P. Dunne, R. J. Stouffer, J. G. John, Reductions in labour capacity from heat stress under climate warming. *Nat. Clim. Chang.* **3**, 563–566 (2013).
3. R. Thompson, R. Hornigold, L. Page, T. Waite, Associations between high ambient temperatures and heat waves with mental health outcomes: A systematic review. *Public Health* **161**, 171–191 (2018).
4. A. M. Rizwan, L. Y. C. Dennis, C. Liu, A review on the generation, determination and mitigation of urban heat island. *J. Environ. Sci.* **20**, 120–128 (2008).
5. IPCC, "The physical science basis, contribution of working group I to the sixth assessment report of the Intergovernmental Panel on Climate Change," in *Climate Change 2021*, IPCC, Ed. (Cambridge Univ. Press, 2021), pp. 113–119.
6. H. Taha, Urban climates and heat islands: Albedo, evapotranspiration, and anthropogenic heat. *Energy Build.* **25**, 99–103 (1997).
7. S. L. Harlan, D. M. Ruddell, Climate change and health in cities: Impacts of heat and air pollution and potential co-benefits from mitigation and adaptation. *Curr. Opin. Environ. Sustain.* **3**, 126–134 (2011).
8. C. Tuholske, K. Caylor, C. Funk, A. Verdin, S. Sweeney, K. Grace, P. Peterson, T. Evans, Global urban population exposure to extreme heat. *Proc. Natl. Acad. Sci. U.S.A.* **118**, e2024792118 (2021).
9. C. J. Schell, K. Dyson, T. L. Fuentes, S. Des Roches, N. C. Harris, D. S. Miller, C. A. Woelfle-Erskine, M. R. Lambert, The ecological and evolutionary consequences of systemic racism in urban environments. *Science* **369**, eaay4497 (2020).
10. L. W. Clarke, G. D. Jenerette, A. Davila, The luxury of vegetation and the legacy of tree biodiversity in Los Angeles, CA. *Landsc. Urban Plan.* **116**, 48–59 (2013).
11. D. H. Locke, B. Hall, J. M. Grove, S. T. A. Pickett, L. A. Ogden, C. Aoki, C. G. Boone, J. P. M. O'Neil-Dunne, Residential housing segregation and urban tree canopy in 37 US cities. *npj Urban Sustain.* **1**, 15 (2021).
12. J. S. Hoffman, V. Shandas, N. Pendleton, The effects of historical housing policies on resident exposure to intra-urban heat: A study of 108 US urban areas. *Climate* **8**, 12 (2020).
13. T. Chakraborty, A. Hsu, D. Many, G. Sheriff, A spatially explicit surface urban heat island database for the United States: Characterization, uncertainties, and possible applications. *ISPRS J. Photogramm. Remote Sens.* **168**, 74–88 (2020).
14. A. Hsu, G. Sheriff, T. Chakraborty, D. Many, Disproportionate exposure to urban heat island intensity across major US cities. *Nat. Commun.* **12**, 2721 (2021).
15. C. W. Tessum, J. S. Apte, A. L. Goodkind, N. Z. Muller, K. A. Mullins, D. A. Paoletta, S. Polasky, N. P. Springer, S. K. Thakrar, J. D. Marshall, J. D. Hill, Inequity in consumption of goods and services adds to racial-ethnic disparities in air pollution exposure. *Proc. Natl. Acad. Sci. U.S.A.* **116**, 6001–6006 (2019).
16. G. Adamkiewicz, A. R. Zota, M. P. Fabian, T. Chahine, R. Julien, J. D. Spengler, J. I. Levy, Moving environmental justice indoors: Understanding structural influences on residential exposure patterns in low-income communities. *Am. J. Public Health* **101**, S238–S245 (2011).
17. P. Vahmani, G. A. Ban-Weiss, Impact of remotely sensed albedo and vegetation fraction on simulation of urban climate in WRF-urban canopy model: A case study of the urban heat island in Los Angeles. *J. Geophys. Res.* **121**, 1511–1531 (2016).
18. G. Hulley, S. Shivers, E. Wetherley, R. Cudd, New ECOSTRESS and MODIS land surface temperature data reveal fine-scale heat vulnerability in cities: A case study for Los Angeles County, California. *Remote Sens.* **11**, 2136 (2019).
19. J. B. Fisher, B. Lee, A. J. Purdy, G. H. Halverson, M. B. Dohlen, K. Cawse-Nicholson, A. Wang, R. G. Anderson, B. Aragon, M. A. Arain, D. D. Baldocchi, J. M. Baker, H. Barral, C. J. Bernacchi, C. Bernhofer, S. C. Biraud, G. Bohrer, N. Brunsell, B. Cappelaere, S. Castro-Contreras, J. Chun, B. J. Conrad, E. Cremonese, J. Demarty, A. R. Desai, A. De Ligne, L. Foltynová, M. L. Goulden, T. J. Griffis, T. Grünwald, M. S. Johnson, M. Kang, D. Kelbe, N. Kowalska, J.-H. Lim, I. Mainassara, M. F. McCabe, J. E. C. Missik, B. P. Mohanty, C. E. Moore, L. Morillas, R. Morrison, J. W. Munger, G. Posse, A. D. Richardson, E. S. Russell, Y. Ryu, A. Sanchez-Azofeifa, M. Schmidt, E. Schwartz, I. Sharp, L. Šigut, Y. Tang, G. Hulley, M. Anderson, C. Hain, A. French, E. Wood, S. Hook, ECOSTRESS: NASA's next generation mission to measure

- evapotranspiration from the International Space Station. *Water Resour. Res.* **56**, e2019WR026058 (2020).
20. N. C. Parazoo, R. W. Coleman, V. Yadav, E. N. Stavros, G. Hulley, L. Hutyra, Diverse biosphere influence on carbon and heat in mixed urban Mediterranean landscape revealed by high resolution thermal and optical remote sensing. *Sci. Total Environ.* **806**, 151335 (2022).
 21. R. W. Coleman, N. Stavros, G. Hulley, N. Parazoo, Comparison of thermal infrared-derived maps of irrigated and non-irrigated vegetation in urban and non-urban areas of Southern California. *Remote Sens.* **12**, 4102 (2020).
 22. L. Zhao, X. Lee, R. B. Smith, K. Oleson, Strong contributions of local background climate to urban heat islands. *Nature* **511**, 216–219 (2014).
 23. C. D. Ziter, E. J. Pedersen, C. J. Kucharik, M. G. Turner, Scale-dependent interactions between tree canopy cover and impervious surfaces reduce daytime urban heat during summer. *Proc. Natl. Acad. Sci. U.S.A.* **116**, 7575–7580 (2019).
 24. H. Akbari, D. M. Kurn, S. E. Bretz, J. W. Hanford, Peak power and cooling energy savings of shade trees. *Energy Build.* **25**, 139–148 (1997).
 25. C. Daly, M. Halbleib, J. I. Smith, W. P. Gibson, M. K. Doggett, G. H. Taylor, J. Curtis, P. P. Pastoris, Physiographically sensitive mapping of climatological temperature and precipitation across the conterminous United States. *Int. J. Climatol.* **28**, 2031–2064 (2008).
 26. T. Chakraborty, Z. S. Venter, Y. Qian, X. Lee, Lower urban humidity moderates outdoor heat stress. *AGU Adv.* **3**, e2022AV000729 (2022).
 27. E. Litvak, K. F. Manago, T. S. Hogue, D. E. Pataki, Evapotranspiration of urban landscapes in Los Angeles, California at the municipal scale. *Water Resour. Res.* **53**, 4236–4252 (2017).
 28. Y.-J. Chen, J. P. McFadden, K. C. Clarke, D. A. Roberts, Measuring spatio-temporal trends in residential landscape irrigation extent and rate in Los Angeles, California using SPOT-5 satellite imagery. *Water Resour. Manag.* **29**, 5749–5763 (2015).
 29. N. S. Bijkor, H. R. McCarthy, D. Zhang, D. E. Pataki, Water sources of urban trees in the Los Angeles metropolitan area. *Urban Ecosyst.* **15**, 195–214 (2012).
 30. E. Porse, K. B. Mika, E. Litvak, K. F. Manago, T. S. Hogue, M. Gold, D. E. Pataki, S. Pincetl, The economic value of local water supplies in Los Angeles. *Nat. Sustain.* **1**, 289–297 (2018).
 31. X. Huang, D. L. Swain, Climate change is increasing the risk of a California megaflood. *Sci. Adv.* **8**, eabq0995 (2022).
 32. B. F. Sanders, J. E. Schubert, D. T. Kahl, K. J. Mach, D. Brady, A. AghaKouchak, F. Forman, R. A. Matthew, N. Ulibarri, S. J. Davis, Large and inequitable flood risks in Los Angeles, California. *Nat. Sustain.* **6**, 47–57 (2023).
 33. H. Yoonus, S. G. Al-Ghamdi, Environmental performance of building integrated grey water reuse systems based on life-cycle assessment: A systematic and bibliographic analysis. *Sci. Total Environ.* **712**, 136535 (2020).
 34. H. Jeong, O. A. Broesicke, B. Drew, J. C. Crittenden, Life cycle assessment of small-scale greywater reclamation systems combined with conventional centralized water systems for the City of Atlanta, Georgia. *J. Clean. Prod.* **174**, 333–342 (2018).
 35. V. Hasik, N. E. Anderson, W. O. Collinge, C. L. Thiel, V. Khanna, J. Wirick, R. Piacentini, A. E. Landis, M. M. Bilec, Evaluating the life cycle environmental benefits and trade-offs of water reuse systems for net-zero buildings. *Environ. Sci. Technol.* **51**, 1110–1119 (2017).
 36. Los Angeles Department of Water and Power, *Los Angeles Department of Water and Power 2015 Briefing Book* (2015); https://d3n8a8pro7vhmx.cloudfront.net/themes/5595df952213930462000001/attachments/original/1430386934/LADWP_Water_System_Fact_Sheet.pdf?1430386934.
 37. C. Mini, T. S. Hogue, S. Pincetl, Estimation of residential outdoor water use in Los Angeles, California. *Landsc. Urban Plan.* **127**, 124–135 (2014).
 38. M. Santamouris, Cooling the cities – A review of reflective and green roof mitigation technologies to fight heat island and improve comfort in urban environments. *Sol. Energy* **103**, 682–703 (2014).
 39. H. Akbari, S. Menon, A. Rosenfeld, Global cooling: Increasing world-wide urban albedos to offset CO₂. *Clim. Change* **94**, 275–286 (2009).
 40. J. Zhang, K. Zhang, J. Liu, G. Ban-Weiss, Revisiting the climate impacts of cool roofs around the globe using an Earth system model. *Environ. Res. Lett.* **11**, 084014 (2016).
 41. J. Zhang, Y. Li, W. Tao, J. Liu, R. Levinson, A. Mohegh, G. Ban-Weiss, Investigating the urban air quality effects of cool walls and cool roofs in Southern California. *Environ. Sci. Technol.* **53**, 7532–7542 (2019).
 42. A. Middel, V. Kelly Turner, F. A. Schneider, Y. Zhang, M. Stiller, Solar reflective pavements —A policy panacea to heat mitigation? *Environ. Res. Lett.* **15**, 064016 (2020).
 43. A. Witze, Extreme heatwaves: Surprising lessons from the record warmth. *Nature* **608**, 464–465 (2022).
 44. G. C. Hulley, F. M. Götsche, G. Rivera, S. J. Hook, R. J. Freepartner, M. A. Martin, K. Cawse-Nicholson, W. R. Johnson, Validation and quality assessment of the ECOSTRESS level-2 land surface temperature and emissivity product. *IEEE Trans. Geosci. Remote Sens.* **60**, 10.1109/TGRS.2021.3079879, (2021).
 45. K. Li, K. Guan, C. Jiang, S. Wang, B. Peng, Y. Cai, Evaluation of four new land surface temperature (LST) products in the U.S. corn belt: ECOSTRESS, GOES-R, landsat, and sentinel-3. *IEEE J. Sel. Top. Appl. Earth Obs. Remote Sens.* **14**, 9931–9945 (2021).
 46. M. C. Anderson, Y. Yang, J. Xue, K. R. Knipper, Y. Yang, F. Gao, C. R. Hain, W. P. Kustas, K. Cawse-Nicholson, G. Hulley, J. B. Fisher, J. G. Alfieri, T. P. Meyers, J. Prueger, D. D. Baldocchi, C. Rey-Sanchez, Interoperability of ECOSTRESS and Landsat for mapping evapotranspiration time series at sub-field scales. *Remote Sens. Environ.* **252**, 112189 (2021).
 47. G. Baldinelli, S. Bonafoni, A. Rotili, Albedo retrieval from multispectral landsat 8 observation in urban environment: Algorithm validation by in situ measurements. *IEEE J. Sel. Top. Appl. Earth Obs. Remote Sens.* **10**, 4504–4511 (2017).

Acknowledgments

Funding: This study is supported by NASA ECOSTRESS Science Team Project (grant no. 80NSSC20K0078). L.H. thanks the Caltech Resnick Sustainability Institute for supporting her Research Fellowship. **Author contributions:** Y.Y. designed the research. L.H. and Y.Y. collected data and performed analysis. P.O.W. and C.F. contributed to the interpretation of the results. All authors contributed to the writing and editing of the manuscript. **Competing interests:** The authors declare that they have no competing interests. **Data and materials availability:** All data needed to evaluate the conclusions in the paper are present in the paper and/or the Supplementary Materials. The ECOSTRESS data supporting this paper are available in the Caltech Data Repository; <https://data.caltech.edu/records/esx93-qx576> (<https://doi.org/10.22002/esx93-qx576>).

Submitted 12 September 2022

Accepted 28 March 2023

Published 28 April 2023

10.1126/sciadv.ade8501